Electromechanical Resonant Ice Protection Systems: Analysis of Fracture Propagation Mechanisms

Marc Budinger, Valérie Pommier-Budinger, Lokman Bennani, Pierrick Rouset, Elmar Bonaccurso, Fabien Dezitter

Electro-mechanical Resonant Ice Protection Systems: Analysis of Fracture Propagation Mechanisms

Marc Budinger[1]

Institut Clément Ader (ICA), Université de Toulouse, CNRS-INSA-ISAE-Mines Albi-UPS, Toulouse, France

Valérie Pommier-Budinger[2]

Institut Supérieur de l'Aéronautique et de l'Espace de Toulouse (ISAE SUPAERO), Université de Toulouse, France

Lokman Bennani[3]

ONERA, Toulouse, France

Pierrick Rouset[4]

Institut Clément Ader (ICA), Université de Toulouse, CNRS-INSA-ISAE-Mines Albi-UPS, Toulouse, France

Institut Supérieur de l'Aéronautique et de l'Espace de Toulouse (ISAE SUPAERO), Université de Toulouse, France

Elmar Bonaccurso[5]

AIRBUS Central R&T, Munich, Germany

Fabien Dezitter[6]

Airbus Helicopters, Marignane, France

Recent research is showing growing interest in low-power electromechanical de-icing systems and, in particular, de-icing systems based on piezoelectric actuators. These systems use the vibrations generated by piezoelectric actuators at resonance frequencies to produce shear stress at the interface between the ice and the support or to produce tensile stress in the ice. This paper provides analytical and numerical models enabling a better understanding of the main de-icing mechanisms of resonant actuation systems. Different possible ice shedding mechanisms involving cohesive and adhesive fractures are analyzed with an approach combining modal, stress and crack propagation analyses. Simple analytical models are proposed to better understand the effects on ice shedding of the type of mode, ice thickness, or frequency with respect to cohesive and adhesive fractures.

---

[1] Associate professor, INSA Toulouse, Mechanical Engineering Department, marc.budinger@insa-toulouse.fr (corresponding author)

[2] Professor, ISAE-Supaero Toulouse, Department of Aerospace vehicles design and control

[3] Research Engineer, ONERA Toulouse

[4] PhD student, ISAE Toulouse, DCAS and ICA Toulouse research labs

[5] Senior scientist, Airbus central R&T

[6] Senior scientist, Airbus Helicopters

Nomenclature

a	=	length of the beam, m
b	=	depth of plate, m
c_{alu}	=	Young's modulus of the aluminum, Pa
c_{ice}	=	Young's modulus of the ice Pa
f_r	=	resonance frequency, Hz
G	=	strain energy release rate, J.m^{-2}
G_c	=	Critical energy release rate, J.m^{-2}
h_{alu}	=	thickness of the support, m
h_{ice}	=	thickness of the ice, m
h_n	=	position of the neutral line for the flexural mode, m
K	=	modal stiffness, N/m
l_f	=	length of the fracture, m
M	=	modal mass, kg
n	=	number of anti-nodes for the considered mode, -
U_i	=	stored elastic energy, J
$U(x)$	=	in-plane displacements (for extensional modes), m
U_0	=	anti-node magnitude of in-plane displacements (for extensional modes), m
$W(x)$	=	out-of-plane displacements (for flexural modes), m
W_0	=	anti-node magnitude of out-of-plane displacements (for flexural modes), m
v	=	speed of sound, m/s
x	=	transverse position over the beam of length a, m
σ	=	stress, Pa
ε	=	strain, -
ψ	=	rotation of a cross section, rad
π_i	=	dimensionless number, -
ω	=	angular frequency of the considered mode, rad.s^{-1}
ρ_{alu}	=	density of the aluminum, kg.m^{-3}
ρ_{ice}	=	density of the ice, kg.m^{-3}

I. Introduction

ICE accretion on aircraft or rotorcraft can affect control and cause mechanical failures. Icing occurs when an aircraft flies through clouds in which super cooled droplets are suspended in an atmosphere with an ambient air temperature below the freezing point. The droplets impinge on the aircraft surfaces and freeze, leading to ice accretion. The resulting change in the aircraft geometry can modify wing aerodynamic characteristics (loss of lift, increase in drag) or even damage the engine by ice ingestion. Regarding electrical de-icing systems, electro-thermal and electro-impulse technologies are already implemented on aircraft but studies are currently in progress to propose new solutions that consume less energy or have less bulky power supplies. Among these studies, de-icing systems based on piezoelectric systems are a subject of growing interest. The principle is to apply vibrations to the structure that create high-level stresses greater than those required to bring about delamination or cracking of the ice accumulated on the structure [1]. Extensional or flexural modes can be excited and different frequency ranges have been investigated: low frequencies (Hz) [2]..[5], high frequencies (kHz) [6]..[15] and waves (MHz) [16][17]. Paper [18] proposes a computational method for estimating amplitude of vibrations to initiate fractures according to the type of mode (extensional or flexural) and to the frequency range. To go further than the prediction of the initiation of de-icing, more work is required to model and understand what happens after the initial cracks or delamination are generated, and how the cracks or delamination can propagate. The fracture propagation mechanisms in the ice or at the ice/support interface involve cohesive failure (which induces cracks) and adhesive failure (which induces delamination). There are currently no studies that model these mechanisms for electromechanical resonant ice protection systems.

In this article, this problem is studied through numerical simulations, analytical modeling and experimental tests on elementary geometries. The supports chosen for modeling and tests are simple plates in order to promote deeper understanding of the phenomena through analytical models. The objective is to obtain models to guide the design or analyze experimental tests. The article focuses on de-icing mechanisms related to resonance modes and does not address electromechanical coupling.

Section II of this article sums up the state of the art concerning the data and models necessary for further developments. Section III develops the computations, based on stress formulas, for estimating the vibration amplitudes leading to the initiation of de-icing. The computations are made for two criteria based on the tensile strength in the ice and on the shear strength at the ice/support interface. Section IV explains general assumptions and introduces the models used in this paper for estimating fracture propagation once de-icing is initiated. It

highlights two different possible fracture propagation mechanisms, the first initiated by tensile stresses and the second by shear stresses. Sections V and VI study fracture propagation for the two mechanisms introduced previously and for flexural resonance modes only. The last section extends the study to extensional modes and compares flexural and extensional modes for fracture propagation.

II. Modeling of Piezoelectric De-icing Systems: State of the Art

This state of the art is limited to the phenomena, data or modeling methods useful for designing and analyzing de-icing systems activated by modal vibrations. Piezoelectric anti-icing systems [19] or ice accretion characterization systems [20][21] are not considered in this paper.

In order to develop models for the design and analysis of piezoelectric systems, it is interesting to determine the main physical effects involved in de-icing. Many authors have set up video recordings [12][14][22] during their tests. The speed of the fracture phenomena, with time constants lower than milliseconds, is emphasized by the use of fast video cameras. The analyses of the videos highlight two types of phenomena: cracks within the ice (cohesive fracture) and delamination at the ice/support interface (adhesive fracture). The order of appearance of these two phenomena is not always the same [22]: cohesive fracture then adhesive fracture or adhesive fracture then cohesive fracture. The two phenomena can be consecutive without interruption or can require an increase in voltage magnitude or change of frequency to occur after a first fracture. In the tests reported in the literature, the activation of the support is generally carried out by a sweep over the frequency ranges that can excite extensional [6]..[12] or flexural [13]..[15][22] modes. For all of these modes, it is possible to note a change in the resonance frequency with the thickness of the ice and a significant amplification of the vibrations at resonance. The absorbed current and the quality factor may differ depending on the type of mode [23], extensional or flexural.

First of all, modeling requires the characteristics of the ice to be known. Many publications [24]..[31] and research projects [32] deal with this research area. For high strain rate (higher than 10^{-4} s^{-1}), ice exhibits macroscopically brittle behavior [29]. The main characteristics useful for our case of applications are thus Young's modulus, density, shear and tensile strengths, and critical energy release rate. These characteristics vary considerably [20][21][24]..[31] depending on the type of ice (glaze or rime), the means used to obtain this ice (freezer or wind tunnel), the type of degradation (cohesive or adhesive), and the interface material. As glaze ice is best known, Tables 1 and 2 summarize the values of the quantities that are used to carry out the numerical

applications or simulations for this ice type, in this article. These values should only be taken as mean values because the literature presents a great variability of results concerning ice properties.

A number of papers put forward analytical or numerical modeling elements. They consist mostly of numerical modal analyses correlated with experimental identification [15]. They can also take the form of frequency analyses which allow the piezoelectric coupling and the damping levels to be taken into account in order to estimate the stress levels at the ice/support interface [7]. Other papers couple modal analysis and model reduction to obtain these constraints [18][37]. The phenomenon of fracture propagation is rarely discussed in piezoelectric de-icing papers. It is necessary to turn to the modeling of electro-impulse [33] or electro-thermal [34][35][36] de-icing systems to find models taking cohesive or adhesive fractures into account. To study fracture mechanics, different methods can be chosen and are known to give similar results for linear elastic fracture mechanisms: the stress intensity factor approach [34], the cohesive zone model [33] and the energy balance approach [35][36]. The energy balance approach is used in this paper because of its similarity with energy approaches to determine resonance modes. This approach compares the strain energy release rate called G to a critical value G_c: a value of G greater than G_c indicates that a crack can grow. Table 2 gives the critical energy release rates G_c (J/m²) commonly used to predict the ability of glaze ice to resist to cohesive or adhesive fractures.

Table 1 – Ice properties of glaze ice

	Glaze ice
Young's modulus, c_{ice}	9.3 10^9 Pa
Poisson's ratio, γ_{ice}	0.325
Density, ρ_{ice}	900 kg/m3

Table 2 – Strength and critical energy release rate for glaze ice

	Cohesive (glaze ice)	Adhesive (ice/aluminum)
Strength, c_{ice}	3 MPa, for freezer ice	1 MPa, for freezer ice
Critical energy release rate, G_c	1 J/m²	0.5 J/m²

III. Initiation of De-icing

The target of this section is to recall the conditions that lead to an initiation of de-icing [18][37][38]. The support is assumed to be covered by an ice layer of constant thickness made in a freezer. The numerical applications are made for a support thickness of 1.5 mm and an ice layer thickness of 2 mm.

A. Beam Analytical Model

The resonance modes used in the literature for de-icing are essentially in-plane extensional modes and out-of-plane flexural modes. To simplify the analysis, several assumptions are made: support and ice are considered as a thin multilayer beam (1D model). This section summarizes the equations already presented by the authors. For more details on their assumptions and developments, the reader is invited to refer to the corresponding papers [18][37]. Mode shapes are assumed to be identical to that of a uniform beam and boundary conditions are simply supported as in papers [18][37]. Fig. 1 shows the beam under study.

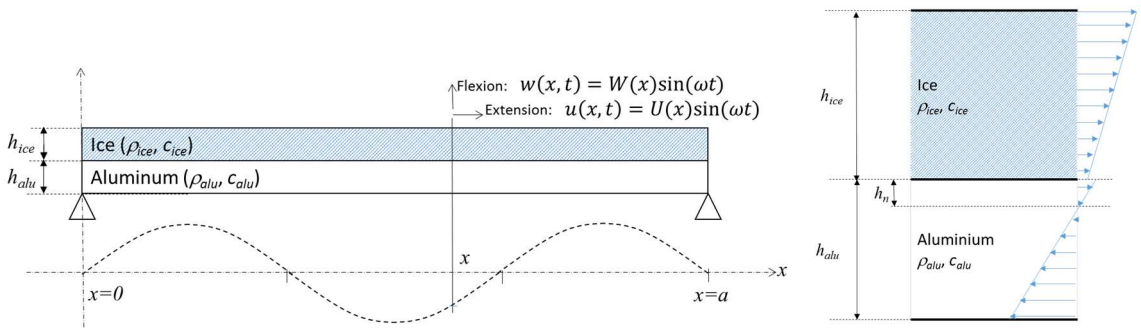

Fig. 1 –Element of the beam under study [18][37]

For flexural modes, the position of the neutral line h_n can be obtained by assuming that the tensile force in a section is zero [39]. This results in:

$$h_n = \frac{1}{2}\frac{c_{alu}h_{alu}^2 - c_{ice}h_{ice}^2}{c_{alu}h_{alu} + c_{ice}h_{ice}} \tag{1}$$

Table 3 synthetizes the analytical formulas derived from previous assumptions to compute strains and stresses in the ice, in the aluminum substrate and at the ice/support interface. The formulas of the peak out-of-plane shear stress were obtained by isolating an element of ice of thickness *dx* subjected to elastic forces, inertial forces and shear forces at the ice/support interface (Fig. 1). The resonance frequencies were obtained by Rayleigh's method using the expression of the strains to estimate the kinetic and potential energies.

Table 3 – 1D modes formulas

	Extensional modes	Flexural modes
Displacement	$u(x,t) = U(x)\sin\omega t = U_0 \sin\frac{n\pi x}{a}\sin\omega t$	$w(x,t) = W(x)\sin\omega t = W_0 \sin\frac{n\pi x}{a}\sin\omega t$ $u(x,t) = -z\frac{\partial w}{\partial x} = U(x)\sin\omega t$
Peak tensile strain	$\varepsilon_x = \frac{\partial U(x)}{\partial x} = U_0\frac{n\pi}{a}cos\frac{n\pi x}{a}$	$\varepsilon_x = \frac{\partial U(x)}{\partial x} = W_0 z\left(\frac{n\pi}{a}\right)^2 sin\frac{n\pi x}{a}$
Peak ice tensile stress in ice	$\sigma_x = c_{ice}\varepsilon_x = c_{ice}U_0\frac{n\pi}{a}cos\frac{n\pi x}{a}$	$\sigma_x = c_{ice}(h_{ice}+h_n)\left(\frac{n\pi}{a}\right)^2 W_0 sin\frac{n\pi x}{a}$
Peak tensile stress in aluminum	$\sigma_x = c_{alu}\varepsilon_x = c_{alu}U_0\frac{n\pi}{a}cos\frac{n\pi x}{a}$	$\sigma_x = c_{alu}(h_{alu}-h_n)\left(\frac{n\pi}{a}\right)^2 W_0 sin\frac{n\pi x}{a}$
Peak shear stress at the ice/support interface	$\tau_{xz} = \left(\rho_{ice}\omega^2 - c_{ice}\left(\frac{n\pi}{a}\right)^2\right)h_{ice}U_0 sin\frac{n\pi x}{a}$	$\tau_{xz} = c_{alu}\left(\frac{n\pi}{a}\right)^3\frac{(h_{alu}-h_n)^2 - h_n^2}{2}W_0 cos\frac{n\pi x}{a}$
Angular frequency	$\omega = \pi\frac{n}{a}\sqrt{\frac{c_{ice}h_{ice}+c_{alu}h_{alu}}{\rho_{ice}h_{ice}+\rho_{alu}h_{alu}}}$	$\omega = \pi^2\left(\frac{n}{a}\right)^2\sqrt{\frac{EI}{\rho_{ice}h_{ice}+\rho_{alu}h_{alu}}}$ with $EI = \frac{c_{alu}}{3}(h_n^3 + (h_{alu}-h_n)^3) + \frac{c_{ice}}{3}((h_n+h_{ice})^3 - h_n^3)$

B. Beam Analytical Models Analysis

These analytical formulas show that, for extensional modes, the maximum tensile stress in the substrate or in the ice is located on the displacement nodes and the maximum shear stress at the ice/support interface is on the displacement antinodes. For flexural modes, the maximum shear stress is located on the nodes and the maximum tensile stress on the antinodes.

The extensional and flexural modes are compared in [18], in particular for their ability to generate stress. For a given frequency and a given displacement, the shear stress level at the ice/support interface and the tensile stress at the top surface of the ice layer are smaller for extensional than for flexural modes. Extensional modes generally appear at higher frequencies (over 15 kHz) and require higher displacements and consequently generally higher power. Thus, to initiate ice delamination or ice fractures while minimizing the displacements (and potentially the consumed power) of the piezoelectric actuators, it is more efficient to excite flexural modes. The set of diagrams in Fig. 2 focuses on the flexural modes and shows, as a function of resonance frequencies:

a) The vibratory magnitude necessary to reach the tensile criterion at the top surface of the ice layer or the shear criterion at the ice/support interface. As higher resonance frequencies entail smaller distances between nodes, higher bending radius and thus higher stresses, the requested magnitudes decrease with frequency. For low frequencies, initiation by crack preferably occurs on the top surface of the ice layer. Initiation by delamination only occurs at higher frequencies. The two phenomena take place simultaneously and cross here at about 40 kHz for an ice layer thickness of 2 mm. For a thickness of 4 mm, the crossing between these two phenomena occurs at approximately 25 kHz.

b) The power per m^2 necessary to create these vibrations; this power depends on the mechanical losses to be compensated. They are here estimated by assuming a mechanical quality factor equal to 30. This conservative value is observed in practice in the worst cases for structures in aluminum alloy [23]. It can be observed that the initiation by tensile criterion can be satisfied with low power, a few tens of W per square meter, at low frequency. However, this power increases with increasing resonance frequencies and varies with the ice layer thickness. A parametric variation on this thickness shows an optimum thickness of approximately 1 mm for the initiation by surface fracture and 4 mm for the initiation of de-icing by delamination at the ice/support interface.

c) The stress in the support, here in the aluminum alloy, should also be taken into account because it can cause a reduction in the lifetime if it is excessive. It is also an image of the constraints that can be found in the piezoelectric actuators. For the tensile criterion, the stress in the support is directly connected to the ice strength

and is thus constant with frequency. For the shear criterion, an increase of the frequency has a positive effect by reducing the stress in the support.

Note: a change in the nature of the ice, e.g. to rime ice with a lower Young's modulus, requires larger vibratory amplitudes in order to initiate the de-icing process and thus higher consumptions and stresses in the support.

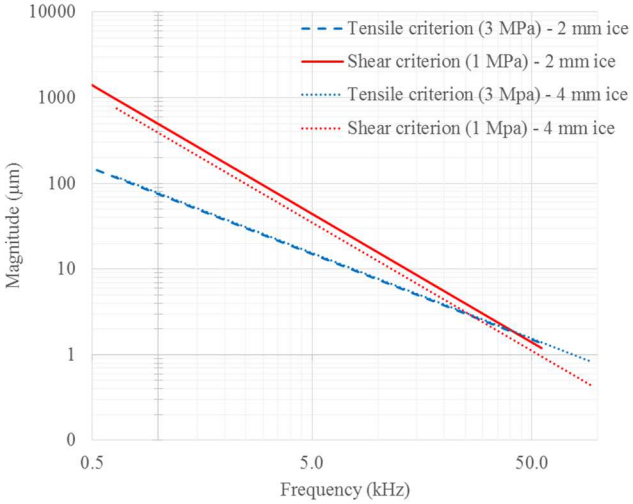

(a) Vibratory magnitude for tensile and shear criteria for different resonant frequencies

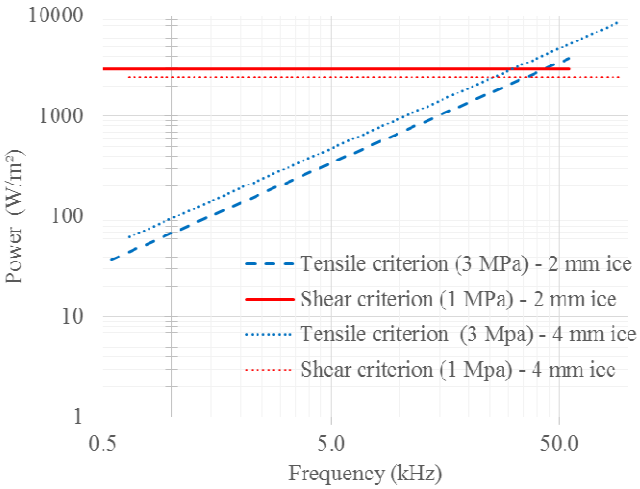

(b) Power per m² for tensile and shear criteria for different resonant frequencies

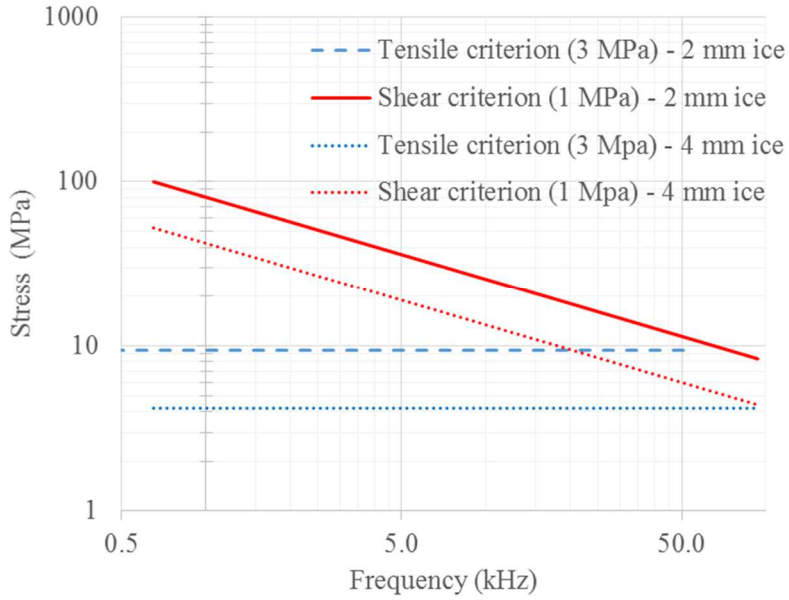

(c) Maximum stress in support for tensile and shear criteria for different resonant frequencies

Fig. 2 – Main values for initiation of de-icing according to tensile and shear criteria

C. Comparison with 3D FEM Models and Experimental Tests

The models of the preceding paragraphs revealed two types of fracture during the initiation of de-icing: cracks on the top surface of the ice layer for low frequencies (caused by tensile stress), and delamination at the ice/support interface for high frequencies (caused by shear stress). These results, established with Bernoulli beam assumptions, are compared here with 3D FEM (Finite Element Method) simulations. The use of particular boundary conditions, symmetry on the antinode and anti-symmetry on the node, allows flexural modes to be simulated on a quarter of a wave-length with a form factor allowing fine meshing. A DoE (Design of Experiments) plan varying the overall dimensions and also the shape factor of the mode (ratio of wavelength in one direction over wavelength in the other direction) resulted in Fig. 4. It can be seen that, despite its great simplicity, the beam model makes it possible to represent the tendency of the amplitude necessary for de-icing initiation according to mechanisms n°1 (tensile criterion) and n°2 (shear criterion).

Finally, different experimental tests were performed to compare simulation results with experimental measurements. The test specimen was an aluminum alloy plate 154 x 52 x 1.5 mm^3 with two piezoelectric ceramics (PIC 151 from Physik Instrumente (PI) GmbH– size: 50 x 25 x 0.5mm^3) bonded in the middle of the plate (Fig. 3). One ceramic was used as the actuator, the other as the sensor. The plate was tested in free conditions with a uniform ice layer (2 mm-thick). This simple structure allows simulation and experimental results to be compared

accurately while limiting uncertainties in the boundary conditions and in the ice profile. The test specimen was tested in a freezer for 3 resonance frequencies (10, 15 and 26 kHz) and 2 types of modes (flexural and extensional). For each resonance mode, sweeps were made around the resonance frequencies while increasing the voltage until the first fractures appeared. The fractures obtained for the three modes are shown in Fig. 3.

The initiation of de-icing for this bare structure and flexural frequencies around 10 kHz and 26 kHz was caused by tensile stresses. Fig. 3(c) represents the mode shape of the corresponding modes where red colors indicate anti-nodes and blue colors indicate nodes. Positions of cracks initiation (red lines of Fig. 3(c)) correspond to positions of anti-nodes. The vibratory magnitudes needed to obtain initiation of the de-icing for these modes are given in Fig. 4 and confirm the orders of magnitude of previous calculations. For the mode at 15 kHz, the initiation of de-icing was also possible with the same order of magnitude because the resonance mode was not purely extensional: as illustrated in Fig. 3(c) for the "extensional mode" at 15 kHz, in addition to in-plane displacements, out-of-plane displacements are also present because of non-uniformity in the thickness of the aluminum-ice composite beam. These tests and other tests for other boundary conditions (clamped) and other forms (leading edge) in an icing wind tunnel are described in greater detail in Pommier-Budinger [38]. They confirm that:

- for flexural modes, the tensile criterion dominates at low frequencies for de-icing,
- extensional modes, which are mainly high frequency, show better properties for delamination,
- the order of magnitude of the vibratory amplitudes that initiate de-icing can be determined from the evaluation of linear stresses.

(a) Test specimen

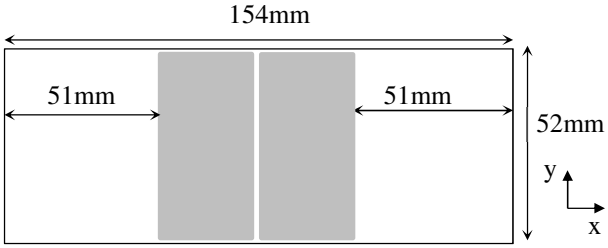

(b) Geometry

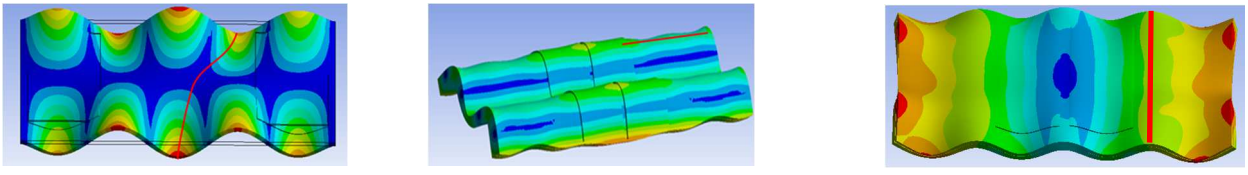

Flexural 10 kHz | Flexural 26 kHz | "Extensional" 15 kHz

(c) Modes tested (blue = node, red = anti-node)

Fig. 3 – Experimental tests

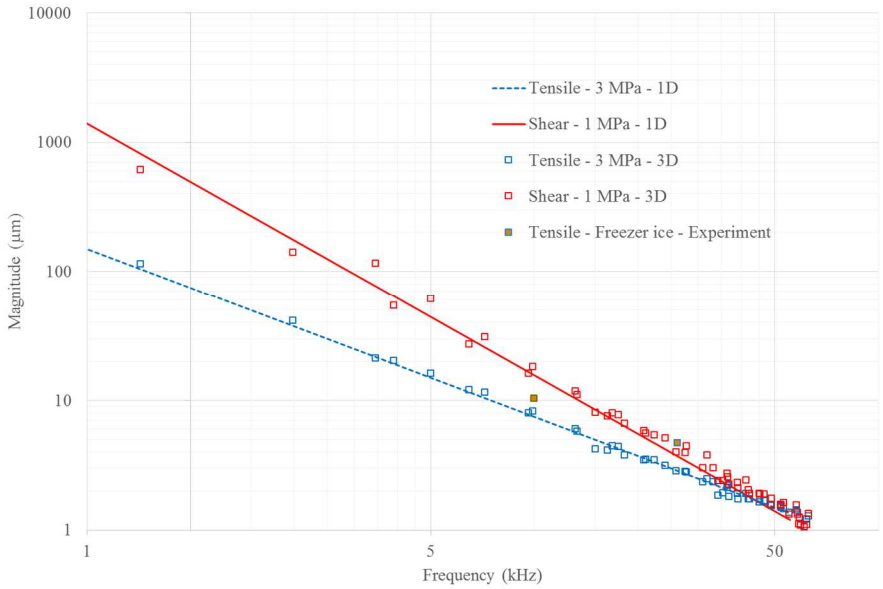

Fig. 4 – Comparison of 1D models (for flexural modes) with numerical (3D FEM) and experimental tests

IV. Fracture Propagation: Assumptions, Methods and Configuration Studied

A. Method and Assumptions for Analysis of Fracture Propagation

In order to study the propagation of fractures, the classical Griffith energy balance approach [40] is used. In the energy balance approach, it is assumed that a certain amount of energy is absorbed by the structure during the formation of an area of fracture surface. When the fracture propagates, a certain amount of stored elastic energy is released. The fracture grows in an unstable way if the released energy is equal to or greater than the absorbed energy.

The strain energy release rate is evaluated by the formula:

$$G = -\frac{1}{b}\left(\frac{dU_i}{dl_f}\right)_{disp} \quad (2)$$

with b the depth of the plate, U_i the stored elastic energy, and l_f the length of the fracture (Fig. 5). The strain energy release rate is compared with fracture toughness values given in Table 2 to conclude on the rapid propagation of cracks or delamination.

The fracture propagation direction is assumed to be known so that the propagation can be studied. It is also assumed here that the fractures take place for vibrations of constant amplitude (*disp* in equation (2) meaning constant displacement) and that the influence of the kinetic energy can be neglected in the energy balance. In order to verify that the modeling can be placed in a quasi-static framework, the execution time of these fracture phases has to be estimated and compared to the vibration period. This evaluation can be made using the speed of fracture propagation at the fracture tip. In ice, the literature [40] estimates this speed at between 20% and 40% of the speed of sound (defined by $v = \sqrt{c/\rho}$), thus about s = 1000 m/s. At the ice/support interface, it is assumed that the speed is of the same order of magnitude. The order of magnitude of the time (in µs) necessary to create a crack through the thickness of the ice layer or to delaminate a part of the ice/support interface is negligible up to about 40 kHz (less than 1/10 of a half-period) if the delamination of the surface is limited to 25%. Finally, it is assumed that the variation in compliance of the structure necessary for the energy approach can be evaluated via a modal analysis.

B. Configurations Studied

Fig. 5 describes the four configurations that are studied in the next sections. They enable comparisons to be made for:

- the type of excited mode: flexion or extension.
- the mechanism of initiation of fracture: tensile stress on the surface of the ice (mechanism n°1) or shear stress at the ice/support interface (mechanism n°2).

The objective of this work is to obtain analytical models of the fracture propagation in order to evaluate the potential of each case for de-icing. The phases of cohesive fracture and adhesive fracture in mechanism n°1 are modeled independently, without analyzing either the switch from cohesive fracture to adhesive fracture or the end of delamination.

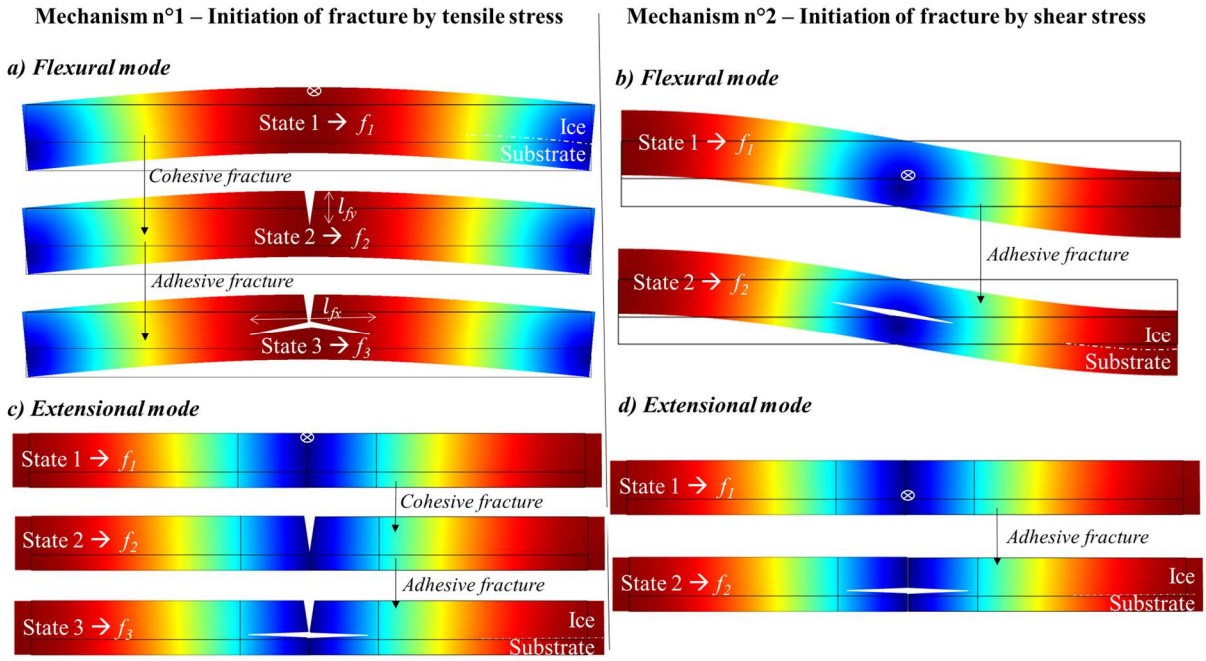

Fig. 5 – Configurations studied

C. Numerical Study of Fracture with Modal Analysis

As an example of the approach followed to study fracture propagation, the propagation of a cohesive fracture (or crack) according to crack length l_{fy} in the ice thickness is investigated for flexural modes of a beam (Fig. 5(a)). The computations are run for a quarter of wavelength configuration thanks to symmetric and anti-symmetric boundary conditions. The crack is located on an anti-node, starting from the top surface of the ice layer, and the simulations are run for different crack lengths l_{fy} assuming free boundary conditions for the crack. The number of elements along thickness is selected (30-50) in order to ensure a good representation of shear stress. The stored energy is calculated at the resonance frequencies with FEM modal analysis. The FEM modal analysis also allows the stresses and deformations to be computed (Fig. 6).

Fig. 7 summarizes the simulation results for a half wavelength of 30 mm. The initial resonance frequency before crack propagation (l_{fy} = 0 mm) is 6.45 kHz. At the end of the cohesive fracture propagation (l_{fy} = 2 mm), the resonance frequency falls to 5.3 kHz. Fig. 7(a) shows the evolution of the elastic energy as a function of the crack length and for a vibratory amplitude, W_0 = 11 µm (computed with formulas of section III), enabling the fracture to initiate in the ice. The derivation of this energy gives the energy release rate (Fig. 7(b)) and can be compared to the fracture toughness of the ice (1 J/m², value introduced in Table 2 and represented by the red line on Fig. 7(b)). It can be seen that the length of the crack started by the initial vibratory amplitude must be over a certain critical

length to enable unstable propagation of the cohesive fracture. Furthermore, the cracking can also stop if the energy release rate is not sufficient. The complete fracture process may therefore require an increase of the initial vibratory amplitudes calculated in the preceding section on the sole criterion of tensile strength. For this case, a vibratory magnitude W_0 = 15.5 µm initiates a crack length that generates an unstable crack growth through the whole thickness.

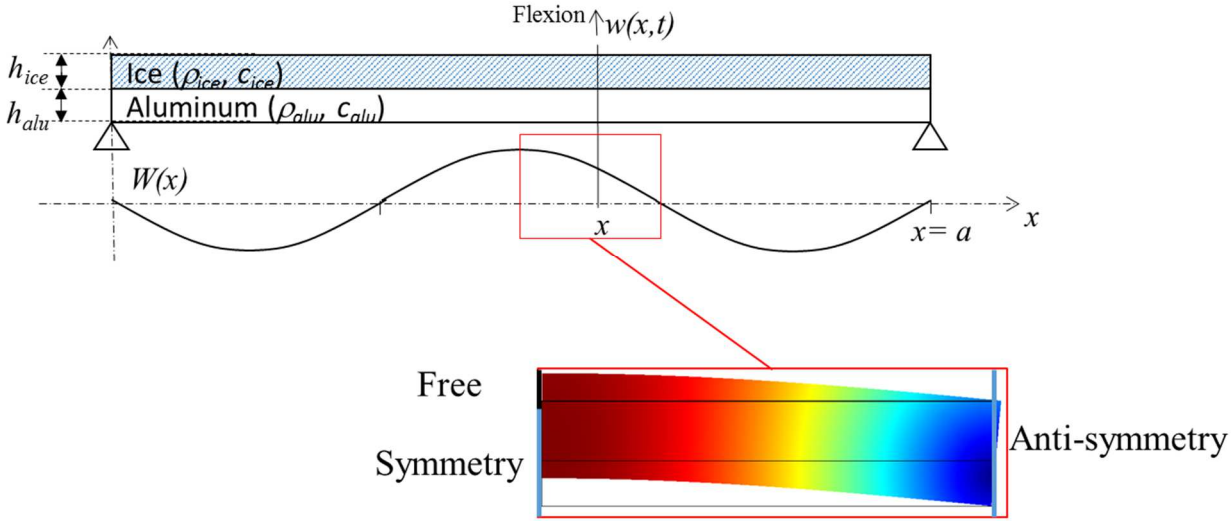

Fig. 6 –2D geometry studied and displacements obtained for a quarter wavelength by modal analysis

Note: the analysis is performed for a cohesive fracture in the ice here but the same type of analysis can be conducted for an adhesive fracture at the ice/support interface.

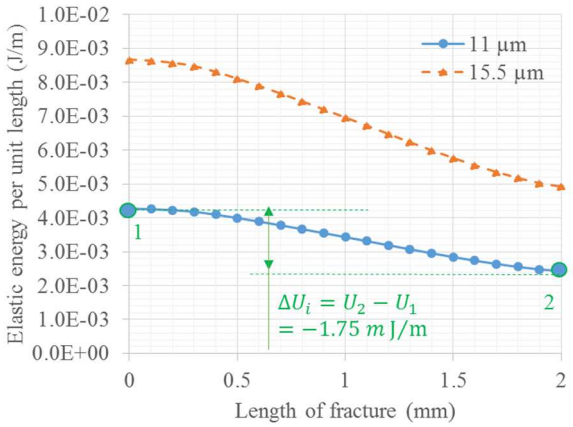

(a) Elastic energy per unit length computed for W_0 = 11 µm and W_0 = 15.5 µm

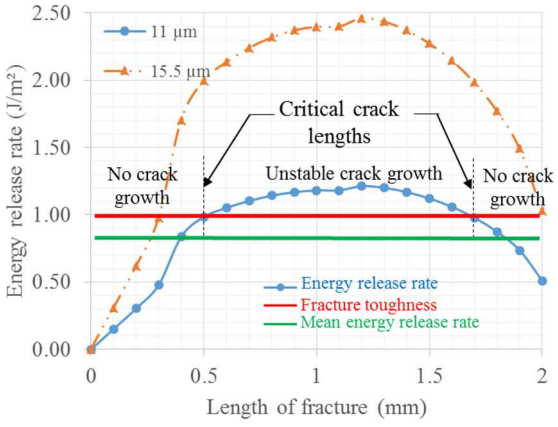

(b) Energy release rate computed for W_0 = 11 µm and W_0 = 15.5 µm

Fig. 7 – Elastic energy and energy release rate during cohesive fracture

The next developments in the paper aim to approximate the mean energy release rate (green line of Fig. 7(b)) for different de-icing configurations.

V. Analysis of Fracture Propagation with Mechanism n°1, Corresponding to Flexural Modes and Tensile Criterion

A. Study Case and Objective of the Study

An analysis of the de-icing tests for flexural modes (Endres [22]) revealed two kinds of fracture propagation, either cohesive and then adhesive, or adhesive and then cohesive. Here, we study the case corresponding to flexural modes represented in Fig. 5(a) and illustrated by the photograph of Fig. 8:

- firstly, cohesive in the ice, just after the initiation of the fracture at the top surface of the ice layer and on the antinode of vibrations.
- secondly, adhesive at the ice/support interface, starting from the base of the fracture initiated just before. It is often necessary to increase the voltage level to make this appear.

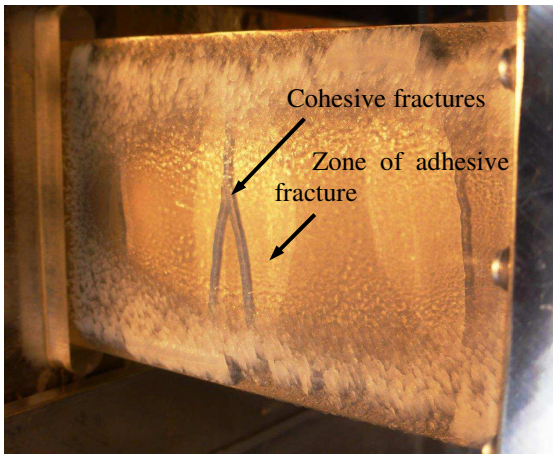

Fig. 8 – Example of cohesive and adhesive fractures for a flexural resonance mode

The first objective here is to determine simplified analytical models describing the cohesive fracture in the ice layer and the adhesive fracture at the ice/support interface, and allowing the elastic energy of the structures to be computed for different configurations of fracture propagation. These models are then used to compute the energy release rate according to the frequency, which can help to analyze the efficiency of de-icing systems using flexural modes and tensile stress.

A simplification is made to obtain these models. The elastic energy is evaluated for only 3 states (Fig. 5(a)):

- state 1: before the cohesive fracture (no fracture in the ice),
- state 2: at the end of the cohesive fracture (crack of the ice through the entire ice layer),
- state 3: at the end of the adhesive fracture (25% of delamination).

We can find a mean value of the mean energy release rate between these states using the relation:

$$G = -\frac{1}{b}\frac{dU_i}{dl_f} \approx -\frac{1}{b}\frac{\Delta U_i}{\Delta l_f} \tag{3}$$

The two mean energy release rates computed between these three states make it possible to evaluate the cohesive and adhesive fracture potentials. As an example, in Fig. 7(a), the cohesive fracture between states 1 and 2 is characterized by a mean value of G of 0.875 J/m² (value computed for $\Delta l_f = 2\text{mm}$ and $\Delta U_i = U_2 - U_1 = -1.75\ m\text{J/m}$) . This value is a simple but interesting indicator of the fracture potential of the configuration: with a value of 0.875 J/m² - lower than but close to 1 J/m² - some cohesive fractures can occur but cannot propagate through the entire ice layer.

B. Analytical Computations of the Elastic Energy and Mean Energy Release Rate

The analytical expression of the elastic energy of state 1, i.e. of the structure without fracture, is obtained using the equations of deformation (Table 3):

$$U_i = \iiint \frac{1}{2}\sigma\varepsilon dv = \iint \frac{1}{2}cy^2\left(\frac{\partial\psi}{\partial x}\right)^2 bdxdy \tag{4}$$

with σ the stress, ε the strain, and ψ the rotation of a cross section.

$$U_{i,1} = \frac{1}{2}\left(\frac{c_{alu}}{3}(h_n^3 + (h_{alu} - h_n)^3) + \frac{c_{ice}}{3}((h_n + h_{ice})^3 - h_n^3)\right)\left(\frac{n\pi}{a}\right)^4 \frac{a}{2n} bW_0^2 \tag{5}$$

The analytical expressions for states 2 and 3 are obtained using a substitution model based on the VPLM (for Variable Power Law Meta-model) method proposed by Sanchez [41]. The approach uses response surface models in logarithmic space combined with dimensional analysis. For the problem considered here, the physical variables involved are:

$$U_{i,2\ or\ 3}/{W_0}^2 = f\left(h_{ice}, h_{alu}, a_n = \frac{a}{n}, c_{ice}, c_{alu}\right) \quad (6)$$

with h_{ice}, h_{alu} the thicknesses of the ice and the support, respectively, a_n the length between 2 nodes, and c_{ice}, c_{alu} the elasticity of the ice and the support, respectively.

With 5 dimensional variables involving 2 physical dimensions, the application of the Buckingham theorem results in 3 dimensionless variables to express the problem. Moreover, the evolution of the resonance frequency is related to the variation in stiffness and therefore to the elastic energy of the structure. If it is assumed that the modal mass and the vibratory amplitude vary little during fracturing, there is a similarity of evolution between resonance frequency and elastic energy:

$$U_i = \frac{1}{2} K W_0^2 \propto f_r^2 \quad (7)$$

where

$$f_r = \frac{1}{2\pi}\sqrt{\frac{K}{M}} \quad (8)$$

with K the modal stiffness and M the modal mass of the resonance mode.

Thus the problem can be rewritten in the following form:

$$\pi_0 = \frac{U_{i,2\ or\ 3}}{U_{i,1}} = \frac{f_{r,2\ or\ 3}^2}{f_{r,1}^2} = f\left(\pi_1 = \frac{h_{ice}}{h_{alu}}, \pi_2 = \frac{h_{alu}}{a_n}, \pi_3 = \frac{c_{ice}}{c_{alu}}\right) \quad (9)$$

Obtaining π_0 only requires the resonance frequencies to be calculated for the three states of the configuration: $f_{r,1}$ for the initial state without fracture, $f_{r,2}$ after cracking on the entire thickness, $f_{r,3}$ after delamination of 25% of the surface. The VPLM method [41] and its associated computer DoE plans [42] are used to obtain the approximate analytical expressions of π_0 for states 2 and 3. The experimental plan to be generated involves the dimensional physical variables $h_{ice}, h_{alu}, a_n, c_{ice}, c_{alu}$ and the dimensionless numbers π_1, π_2, π_3. It contains 4 levels for each dimensionless number, which makes 64 points for this experimental plan. The variation ranges of the variables of the problem are given in Table 4.

Table 4 – Variation range for the DoE

Variables	Units	Variation range
h_{ice}	mm	$0.5 - 5$
h_{alu}	mm	$0.3 - 3$
a_n	mm	$15 - 120$
c_{ice}	GPa	$3 - 10$
c_{alu}	GPa	$10 - 210$
$\pi_1 = h_{ice}/h_{alu}$	-	$1.67\ 10^{-1} - 1.67\ 10^{1}$
$\pi_2 = h_s/a_n$	-	$2.50\ 10^{-3} - 2\ 10^{-1}$
$\pi_3 = c_{ice}/c_{alu}$	-	$1.43\ 10^{-2} - 1$

The variation domains defined above can lead to certain unrealistic configurations such as resonance frequencies of the support that are too low and structures that are too fine. An additional constraint, resulting from the calculation of flexural resonance frequency is then added to the problem under study:

$$\frac{h_{alu}}{a_n^2} > \frac{2}{120^2} \tag{10}$$

The expression of the energy after cohesive fracture

$$\pi_{0,2} = U_{i,2}/U_{i,1} \tag{11}$$

obtained by the regression method is given by:

$$\pi_{0,2} = \cdots$$

$$\ldots k.\pi_1^{a_1+b_{12}\,log(\pi_2)+b_{11}\,log(\pi_1)+b_{13}\,log(\pi_3)+c_{121}\,log(\pi_2)\,log(\pi_1)+c_{111}\,log(\pi_1)\,log(\pi_1)+c_{131}\,log(\pi_3)\,log(\pi_1)} \tag{12}$$

$$\ldots \pi_2^{a_2+c_{231}log(\pi_3)log(\pi_1)+b_{23}log(\pi_3)}\pi_3^{a_3}$$

with

k = 0.21669, a_1 = -1.7066, a_2 = -0.31725, a_3 = -0.33617, b_{12} = -0.68082, b_{11} = -1.4732, b_{13} = -0.63382, c_{121} = -0.36705, c_{111} = -0.43055, c_{231} = -0.21696, c_{131} = -0.25796 and b_{23} = -0.15783.

The expression of the energy after adhesive fracture

$$\pi_{0,3} = U_{i,3}/U_{i,1} \tag{13}$$

obtained by the regression method is given by:

$$\pi_{0,3} = k.\pi_1^{a_1+b_{13}\log(\pi_3)+b_{11}\log(\pi_1)}\pi_2^{a_2}\pi_3^{a_3+b_{33}\log(\pi_3)+c_{331}\log(\pi_3)\log(\pi_1)} \tag{14}$$

with

k = 0.16234, a_1 = -1.385, a_2 = -0.064263, a_3 = -0.52435, b_{13} = -0.30152, b_{11} = -0.79995, b_{33} = -0.092924, c_{331} = 0.12912.

These functions have less than 5% average error over the range of study when they are compared to the simulation data. The use of these functions makes it possible to evaluate the evolution of the mean energy release rate, *G,* as a function of frequency for the cohesive fracture (Fig. 9) and the adhesive fracture (Fig. 10). These evaluations were made for vibratory amplitudes leading to the initiation of de-icing under tensile stress with freezer-type ice (tensile strength of 3 MPa). The evolution of the curves for other strength or amplitude values can be performed by square scaling.

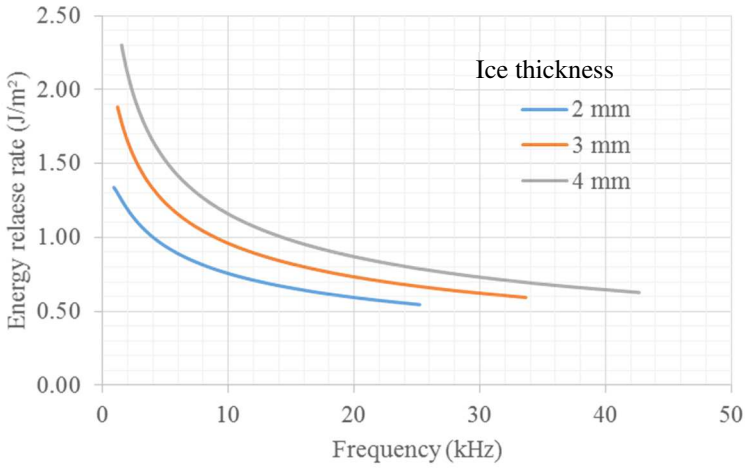

Fig. 9 – Estimated mean energy release rate, *G*, between state 1 and state 2 for cohesive fracture and flexural modes regarding tensile criterion (aluminum 1.5 mm, glaze ice of different thicknesses)

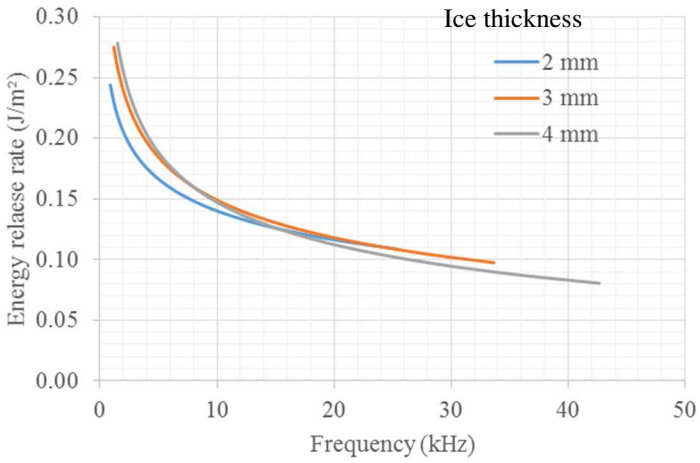

Fig. 10 – Estimated mean energy release rate, *G*, between state 2 and state 3 for adhesive fracture and flexural modes regarding tensile criterion (aluminum 1.5 mm, glaze ice of different thicknesses)

C. Analysis of Results

The analysis of the curves of Fig. 9 and Fig. 10 leads to the following remarks for the de-icing with flexural modes and tensile stress:

- The evolution of these curves as a function of frequency shows that the increase in frequency makes cohesive or adhesive fracturing more difficult;
- A comparison of the values of G with the values of G_c of the state of the art (Table 2) shows that, using the amplitude computed to initiate the fracture, it is possible to make a cohesive fracture grow on the entire ice layer for low frequencies (on Fig. 9, the values of G are greater than 1 J/m² only for low frequencies) but that it is unlikely to make an adhesive fracture grow at the ice/support interface whatever the frequency (on Fig. 10, the values of G are always smaller than 0.5 J/m²). This point corroborates the experimental results, which showed that the propagation of adhesive fractures required higher supply voltage and thus higher power supply in comparison with the voltage or power required for initiating cohesive fractures.
- The variation of ice thickness affects cohesive fractures more strongly: a thick ice layer strongly facilitates a cohesive fracture but has little effect on an adhesive fracture.

VI. Analysis of Fracture Propagation with Mechanism n°2 Corresponding to Flexural Modes and Shear Criterion

Section III of this paper introduces the possibility of a second de-icing mechanism, illustrated on Fig. 5(b), which should appear for higher frequencies than mechanism n° 1: at a vibration node, shear stresses induce a beginning of delamination. Here, we study the propagation of this adhesive fracture at the ice/support interface, using the methodology introduced in sections IV and V where the elastic energy is now evaluated for only 2 states:

- state 1: before the adhesive fracture (no fracture in the ice),
- state 2: at the end of the adhesive fracture on 25% of the ice/support interface surface.

The first point is identical to that of the previous section and the evaluation of the second point using a substitution model leads to the expression for the energy after adhesive fracture according to the substitution model:

$$\pi_{0,2} = U_{i,2}/U_{i,1} = k.\pi_1^{a_1}\pi_2^{a_2}\pi_3^{a_3} \quad (15)$$

with k = 0.92072, a_1 = -0.024018, a_2 = -0.0048137 and a_3 = -0.010926.

Fig. 11 also compares the energy release rate, G, for adhesive fractures of mechanisms n°1 and n°2, for the same vibratory amplitude levels. It can be seen that mechanism n°2 has a lower fracture potential and unstable delamination growth is even more unlikely when only the vibration amplitude that initiates the fracture is used. Higher vibratory amplitude is required to lead to delamination.

The set of pictures from FEM simulations (Fig. 12) makes it possible to understand the difference in energy release rate, *G,* between the mechanisms n°1 and n°2. These FEM results show the distribution of tensile stresses, shear stresses and stored elastic energy for a bending mode. The spatial zones with high tensile stresses correspond to zones with high stored energy, while zones with high shear stresses correspond to low stored energy. From an analysis of Fig. 11 and Fig. 12, one can understand that fractures of ice occur more easily in zones with high elastic energy. In conclusion, unstable delamination growth through mechanism n° 2 has a low probability.

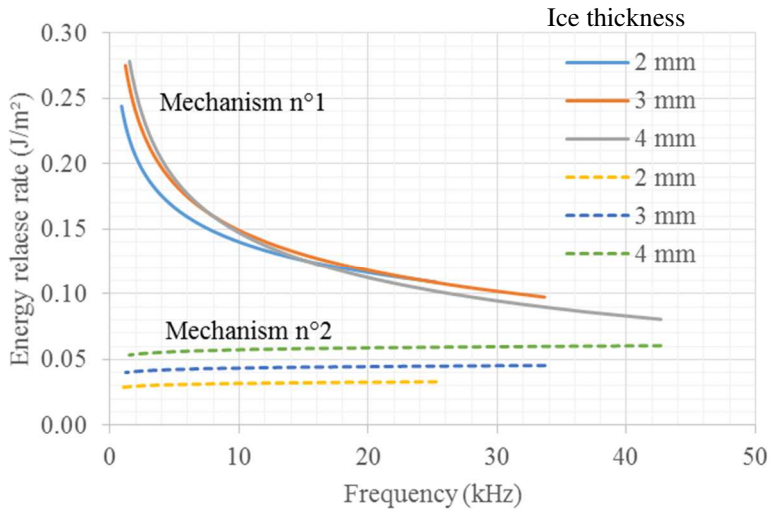

Fig. 11 – Estimated energy release rate, *G*, for adhesive fracture and flexural modes (between state 2 and state 3 for mechanism n°1 (tensile criterion) and between state 1 and state 2 for mechanism n°2 (shear criterion)

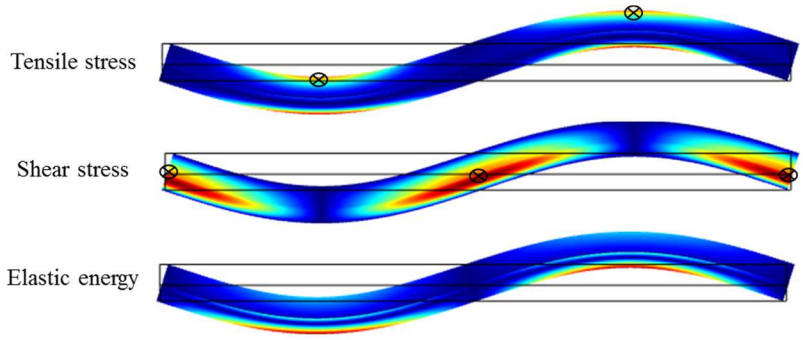

Fig. 12 – Tensile stress, shear stress and elastic energy distribution for a flexural mode

VII. Analysis of Fracture Propagation for Coupled Modes with Extension and Flexion and for Tensile and Shear Criterion

As illustrated in Fig. 3(c), the experiment shows greater delamination for modes having a mixture of displacements in the in-plane (extension) and out-of-plane (flexion) directions. The calculations of section III show that the initiation of delamination is mainly due to the out-of-plane components of these coupled modes. This

section thus focuses on the effect of in-plane deformations on fracture propagation for the two types of mechanisms presented previously.

For the FEM simulations, in order to quantify only the effect of the vibratory components in the plane, boundary conditions are forced on the faces so as to have only extension movements. In order to quantify the maximum effect that can be achieved by these components, the de-icing initiation point is placed at the most favorable position in terms of elastic energy, i.e. at the node of the extensional mode. By taking the approach of sections IV and V, the elastic energy is computed at several points:

- For mechanism n°1 (Fig. 5(c), tensile criterion), with 3 states: initial energy without fracture (state 1), after cohesive fracture in the entire ice layer thickness (state 2), after adhesive fracture on 25% of the ice/support interface (state 3).
- For mechanism n°2 (Fig. 5(c), shear criterion), with 2 states: initial energy without fracture (state 1), after adhesive fracture on 25% of the ice/support interface (state 2).

The cohesive fracture is thus studied between states 1 and 2 of mechanism n°1, and the adhesive fracture between state 2 and state 3 for mechanism n°1 (after a first cohesive fracture) and between state 1 and state 2 for mechanism n° 2 (without initial cohesive fracture).

As previously, the analytical expression for the elastic energy of state 1 (structure without fracture), is obtained using the equations of deformation (Table 3):

$$U_{i,1} = \iiint \frac{1}{2}\sigma\varepsilon dv = \frac{1}{2}\left(c_{alu}h_{alu} + c_{ice}h_{ice}\right)\left(\frac{n\pi}{a}\right)^2 \frac{a}{2n} b U_0^2 \tag{16}$$

The analytical expressions for the other states are obtained, as in Sections IV and V, using substitution models of FEM simulations. To generate the DoE, the ranges of the ice layer thickness and of the ice and support Young's moduli are the same as previously. To have a similar frequency range, however, it is necessary to adapt the range of the wavelength. The parameter a_n (distance between 2 nodes) considered here varies between 50 and 300 mm.

The simulation and meta-modeling results are as follows:

- For cohesive fracture through mechanism n° 1 (Fig. 5(c)): state 2 is very close in energy to the initial state 1. This means that extensional modes cannot be used as an enabler of cohesive fracture. If a crack appears

before delamination in a de-icing process, it is more likely caused by out-of-plane displacements (and thus flexural modes).

- For adhesive fracture through mechanism n° 1 (Fig. 5(c)): the energy release rate for extensional modes (Fig. 13) is higher than for pure flexural modes (Fig. 10). The two diagrams are drawn with the assumption of an equal vibratory magnitude. The beneficial effect increases with the ice layer thickness. The elastic energy stored at the ice/support interface around extensional modes certainly explains the difference of fracture propagation between the purely flexural and combined extensional-flexural modes.
- For adhesive fracture through mechanism n°2 (Fig. 5(d)): as illustrated in Fig. 13, the energy release rate for extensional modes is low in this configuration. Considering this and previous results, de-icing due to mechanism n° 2 and resulting in fast delamination is less likely to occur than delamination due to mechanism n°1.
- Unlike the energy release rate for flexural modes, that for extensional modes is independent of frequency and thus can be helpful for high frequency de-icing.

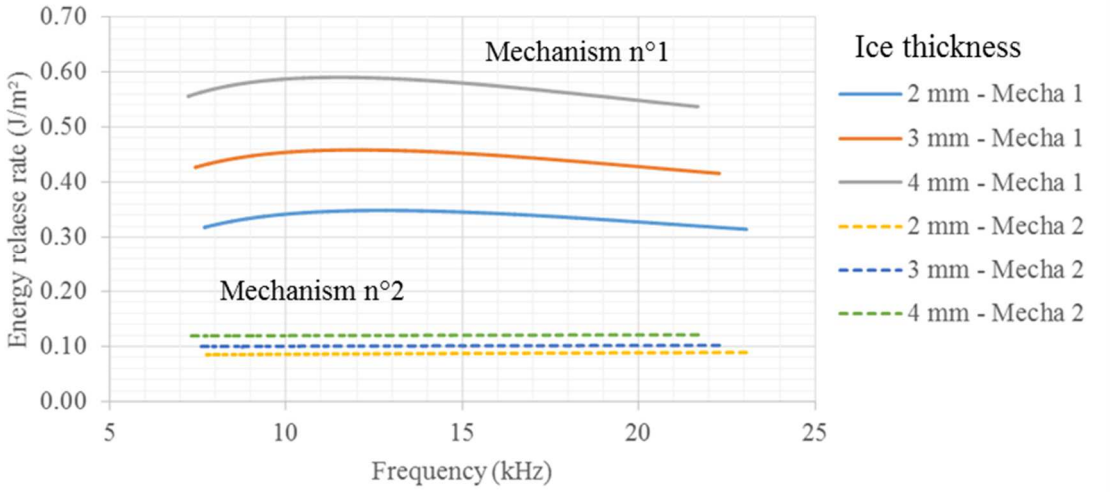

Fig. 13 –Estimated energy release rate, *G*, for adhesive fracture and extensional modes between state 2 and state 3 for mechanism n°1 (tensile criterion) and between state 1 and state 2 for mechanism n°2 (shear criterion)

VIII. Conclusion

The objective of this paper was to set up simplified models for a better understanding of fracture propagation in electromechanical vibratory de-icing systems. To achieve this, various simplifying hypotheses have been used: geometries assimilated to composite beams (support/ice), decoupling of resonance modes (flexion/extension), etc. A first study concerned the initiation of fractures for de-icing. Models and experimental results show that the initiation of fractures can occur at low frequency using tensile stress or at high frequency using shear stress. The study highlights that the flexural modes are the most suitable to initiate fractures.

Using the vibratory amplitude to initiate de-icing as a starting point, a second study concerned fracture propagation. An examination of experimental tests highlighted two possible mechanisms for the propagation: one mechanism initiated by tensile stresses and the other by shear stresses. Several proposals have been made for developing models of fracture propagation: energy balance analysis with modal analysis, simplification of the approach by studying the frequency of resonance on some characteristic states, establishing analytical formulations using substitution models. These analytical models made it possible to carry out trend studies, which revealed: the easier propagation of cohesive fractures for low frequency flexural modes, the low probability of de-icing by shear stress, the importance of the presence of elastic energy at the ice/support interface to generate delamination, and the interest of extensional modes to achieve such delamination. These results can be used as design guidelines for new de-icing architectures. They could be extended by further numerical studies not requiring the fracture propagation direction and by studies on more complex geometries, such as plates or leading edges.

Acknowledgements

The present work is partially funded by Toulouse University and Occitanie region. The authors gratefully acknowledge the support of Florent Huet and Marc Wetterwald from Airbus Operation SAS in Toulouse, without which the present study could not have been completed.

References

[1] Seppings, R. A. (2006). *Investigation of ice removal from cooled metal surfaces* (Doctoral dissertation, Imperial College London (University of London)).

[2] Venna, S. V., & Lin, Y. J. (2002). In-Flight De-Icing Self-Actuating Wing Structures with Piezoelectric Actuators. In *Proceedings of American Society of Mechanical Engineers/International Mechanical Engineering Congress and Exposition* (pp. 237-245).

[3] Venna, S. V., & Lin, Y. J. (2003). Development of Self-Actuating In-Flight De-Icing Structures with Power Consumption Considerations. In *Proceedings of the American Society of Mechanical Engineers International Mechanical Engineering Congress and Exposition 2003* (pp. 45-53).

[4] Venna, S. V., & Lin, Y. J. (2006). Mechatronic development of self-actuating in-flight deicing structures. *IEEE/ASME Transactions on Mechatronics*, *11*(5), 585-592. DOI: 10.1109/TMECH.2006.882990

[5] Venna, S. V., Lin, Y. J., & Botura, G. (2007). Piezoelectric transducer actuated leading edge de-icing with simultaneous shear and impulse forces. *Journal of Aircraft*, *44*(2), 509-515. DOI : 10.2514/1.23996

[6] Palacios, J. L. (2008). Design, fabrication, and testing of an ultrasonic de-icing system for helicopter rotor blades. The Pennsylvania State University.

[7] Palacios, J., Smith, E., & Rose, J. (2008, April). Investigation of an ultrasonic ice protection system for helicopter rotor blades. In *Annual Forum Proceedings-American Helicopter Society* (vol. 64, no. 1, p. 609). American Helicopter Society, inc.

[8] Palacios, J., Smith, E., Rose, J., & Royer, R. (2011). Instantaneous de-icing of freezer ice via ultrasonic actuation. *AIAA journal*, *49*(6), 1158-1167. DOI: 10.2514/1.J050143

[9] Palacios, J., Smith, E., Rose, J., & Royer, R. (2011). Ultrasonic de-icing of wind-tunnel impact icing. *Journal of Aircraft*, *48*(3), 1020. DOI: 10.2514/1.C031201

[10] Palacios, J. L., & Smith, E. C. (2005, April). Dynamic analysis and experimental testing of thin-walled structures driven by shear tube actuators. In *46th AIAA/ASME/ASCE/AHS/ASC Structures, Structural Dynamics and Materials Conference. Austin: American Institute of Aeronautics and Astronautics* (pp. 1-14).

[11] Overmeyer, A., Palacios, J. L., Smith, E. C., & Royer, R. (2011). *Rotating testing of a low-power, non-thermal ultrasonic de-icing system for helicopter rotor blades* (No. 2011-38-0098). SAE Technical Paper.

[12] Overmeyer, A., Palacios, J., & Smith, E. (2012). Actuator bonding optimization and system control of a rotor blade ultrasonic deicing system. *AIAA*, *1476*, 23-26.

[13] Strobl, T., Storm, S., Thompson, D., Hornung, M., & Thielecke, F. (2015). Feasibility study of a hybrid Ice protection system. *Journal of Aircraft, 52(6),* 2064-2076. DOI: 10.2514/1.C033161

[14] Strobl, T., Storm, S., Kolb, M., Haag, J., & Hornung, M. (2014, September). Development of a hybrid ice protection system based on nanostructured hydrophobic surfaces. In *29th Congress of the International Council of the Aeronautical Sciences*.

[15] Villeneuve, E., Harvey, D., Zimcik, D., Aubert, R., & Perron, J. (2015). Piezoelectric Deicing System for Rotorcraft. *Journal of the American Helicopter Society*, *60*(4), 1-12. DOI: 10.4050/JAHS.60.042001

[16] Ramanathan, S., Varadan, V. V., & Varadan, V. K. (2000, June). Deicing of helicopter blades using piezoelectric actuators. In *SPIE's 7th Annual International Symposium on Smart Structures and Materials* (pp. 281-292). International Society for Optics and Photonics.

[17] Kalkowski, M. K., Waters, T. P., Rustighi, E. (2015, March). Removing Surface Accretions with Piezo-Excited High-Frequency Structural Waves. In Proc. SPIE 9431, Active and Passive Smart Structures and Integrated Systems 2015, San Diego, California.

[18] Budinger, M., Pommier-Budinger, V., Napias, G., & Da Silva, A. C. (2016). Ultrasonic Ice Protection Systems: Analytical and Numerical Models for Architecture Tradeoff. *Journal of Aircraft*, 680-690. DOI: 10.2514/1.C033625

[19] Li, D., Chen, Z., & Shi, M. (2010). Effect of ultrasound on frost formation on a cold flat surface in atmospheric air flow. *Experimental Thermal and Fluid Science*, *34*(8), 1247-1252. DOI: 10.1016/j.expthermflusci.2010.05.005

[20] Liu, Y., Bond, L. J., & Hu, H. (2017). Ultrasonic-attenuation-based technique for ice characterization pertinent to aircraft icing phenomena. AIAA Journal, 1-8. DOI: 10.2514/1.J055500

[21] Gao, H., & Rose, J. L. (2009). Ice detection and classification on an aircraft wing with ultrasonic shear horizontal guided waves. IEEE transactions on ultrasonics, ferroelectrics, and frequency control, 56(2), 334-344. DOI: 10.1109/TUFFC.2009.1042

[22] Endres, M., Sommerwerk, H., Mendig, C., Sinapius, M., & Horst, P. (2017). Experimental study of two electro-mechanical de-icing systems applied on a wing section tested in an icing wind tunnel. *CEAS Aeronautical Journal*, *8*(3), 429-439. DOI: 10.1007/s13272-017-0249-0

[23] Rouset, P., Budinger, M., Pommier-Budinger, V. (2017, July). Comparison of extensional and flexural modes for the design of piezoelectric ice protection systems. In 7th European Conference for Aeronautics and Space Sciences (EUCASS), Milano, Italia.

[24] Mohamed, A. M. A., & Farzaneh, M. (2011). An experimental study on the tensile properties of atmospheric ice. *Cold regions science and technology*, *68*(3), 91-98. DOI: 10.1016/j.coldregions.2011.06.012

[25] Scavuzzo, R. J., & Chu, M. L. (1987). Structural properties of impact ices accreted on aircraft structures.

[26] Gammon, P. H., Kiefte, H., Clouter, M. J., & Denner, W. W. (1983). Elastic constants of artificial and natural ice samples by Brillouin spectroscopy. Journal of Glaciology, 29(103), 433-460. DOI: 10.3189/S0022143000030355

[27] Nakaya, U. (1958). Visco-elastic properties of snow and ice in Greenland ice cap. Journal of the Faculty of Science, Hokkaido University. Ser. 2, Physics= 北海道大學理學部紀要, 5(3), 119-164.

[28] Struggl, S., Korak, J., & Feyrer, C. (2011, March). A basic approach for wing leading deicing by smart structures. In *SPIE Smart Structures and Materials+ Nondestructive Evaluation and Health Monitoring* (pp. 79815L-79815L). International Society for Optics and Photonics.

[29] Druez, J., Phan, C. L., Laforte, J. L., & Nguyen, D. D. (1979). The adhesion of glaze and rime on aluminum electrical conductors. *Transactions of the Canadian Society for Mechanical Engineering*, *5*(4), 215-220.

[30] Petrovic, J. J. (2003). Review mechanical properties of ice and snow. *Journal of materials science*, *38*(1), 1-6. DOI: 10.1023/A:1021134128038

[31] Riahi, M. M., Marceau, D., Laforte, C., & Perron, J. (2011). The experimental/numerical study to predict mechanical behaviour at the ice/aluminium interface. *Cold Regions Science and Technology*, *65*(2), 191-202. DOI: 10.1016/j.coldregions.2010.09.002

[32] Ice STORM project, Efficient ice protection Systems and simulation Techniques Of ice Release on propulsive systems, European FP7-TRANSPORT, Project ID: 605180

[33] Sommerwerk, H., & Horst, P. (2017). Analysis of the mechanical behavior of thin ice layers on structures including radial cracking and de-icing. *Engineering Fracture Mechanics*. DOI: 10.1016/j.engfracmech.2017.04.038

[34] Zhang, S., El Kerdi, O., Khurram, R. A., & Habashi, W. G. (2012). FEM analysis of in-flight ice break-up. *Finite elements in analysis and design*, *57*, 55-66. DOI: 10.1016/j.finel.2012.03.005

[35] Bennani, L., Villedieu, P., Salaun, M., & Trontin, P. (2014). Numerical simulation and modeling of ice shedding: Process initiation. *Computers & Structures*, *142*, 15-27. DOI: 10.1016/j.compstruc.2014.06.001

[36] Bennani, L., Villedieu, P., & Salaun, M. (2016). A mixed adhesion–brittle fracture model and its application to the numerical study of ice shedding mechanisms. *Engineering Fracture Mechanics*, *158*, 59-80. DOI: 10.1016/j.engfracmech.2016.02.050

[37] Pommier-Budinger, V., Budinger, M., Tepylo, N., & Huang, X. (2016, June). Analysis of piezoelectric ice protection systems combined with ice-phobic coatings. In 8th AIAA Atmospheric and Space Environments Conference, p. 3442.

[38] V. Pommier-Budinger, M. Budinger, P. Rouset, F. Dezitter, F. Huet, M. Wetterwald, E. Bonaccurso. Electro-mechanical Resonant Ice Protection Systems. Initiation of Fractures with Piezoelectric De-icing Systems. submitted to *AIAA Journal.*

[39] Timoshenko, S. (1940). *Strength of materials Part 1*. D. Van Nostrand Co., Inc.

[40] P.J.G. Schreurs. Fracture Mechanics. Lecture notes, course 4A780, Eindhoven University of Technology

[41] Sanchez, F., Budinger, M., & Hazyuk, I. (2017). Dimensional analysis and surrogate models for the thermal modeling of Multiphysics systems. *Applied Thermal Engineering*, *110*, 758-771. DOI: 10.1016/j.applthermaleng.2016.08.117

[42] Hazyuk, I., Budinger, M., Sanchez, F., & Gogu, C. (2017). Optimal design of computer experiments for surrogate models with dimensionless variables. *Structural and Multidisciplinary Optimization*, 1-17. DOI: 10.1007/s00158-017-1683-7